Experimental and theoretical investigation into X-ray shielding properties of thin lead films

M. Vagheian¹*, D. Sardari², S. Saramad¹, D. Rezaei Ochbelagh¹

¹Tehran Polytechnic University (Amirkabir University of Technology), Tehran, Iran
²Azad University, Science and Research Branch, Tehran, Iran

► *Original article*

*Corresponding authors:
Mehran Vagheian, Ph.D.,
E-mail:
mehran.vagheian@gmail.com

ABSTRACT

Background: Among all of the radiations, X-ray has been always the center of attention due to the increasing availability of the X-ray tubes in industry, research institutes and medical centers. In this study, X-ray shielding properties of bulk and nanostructured thin lead films were investigated by means of Monte-Carlo computational and experimental methods, respectively. *Materials and Methods:* The lead samples were fabricated by the Physical Vapor Deposition technique (PVD) with different thickness of 10, 100 and 1000 nm. To investigate the radiation shielding properties of the nanostructured thin films, all of the prepared samples were subjected to the X-ray ranging from 8 to 14 keV. In order to consider the shielding properties of the bulk-structured thin films, the Monte-Carlo MCNPX code was employed. *Results:* The results indicated that, for low X-ray energies, the nanostructured thin lead films attenuate more than bulk-structured samples; however, the difference disappears as film thickness increases to 1000 nm or X-ray energy reaches 14 keV. *Conclusion:* Results imply that the nanostructured thin lead films attenuate more photons than the bulk-structured thin lead films with the same thicknesses.

Keywords: Nanostructured thin lead films, Advanced X-ray shielding design, MCNPX code, Thin lead film characterization.

INTRODUCTION

Among all of the radiations, X-ray radiation has been always the center of attention due to the increasing availability of the X-ray tubes in industry, research institutes and medical centers. Photons of X-ray s can penetrate into the human body and cause cell injury and even cell death enclosing enclosing or shielding the X-ray generating units with a material which resists X-ray penetration, which is a requisite and concerning issue [1-3].

Some recent studies compared the effect of nano-sized and micro-sized materials on the transmission of different X-ray energy beams. In 2013, Noor Azman *et al.* [4, 5], considered and compared the attenuation ability of the nano-sized and micro-sized WO₃ as a filler loading component within the epoxy composites in different X-ray energies. In a similar recent work, the mass attenuation coefficients of pure concrete and WO₃ added concrete with micro-sized and nano-sized particles were considered and compared with each other. It was observed that shielding properties of concrete doped with WO₃ increased. The results of mass attenuation coefficients also showed that the concrete doped with nano-WO₃ significantly improved shielding properties compared to micro-WO₃ [6]. In 2012, Kunzel and Okuno [7] investigated the effect of thickness and concentration of dispersed micro and nano-sized CuO powder within the polymer resin. They showed that the attenuation property of both the nano-sized and micro-sized CuO would increase by increasing the thickness and concentration. The aforementioned investigations additionally indicated a higher

attenuation ability of the nano-sized particles than those of the micro-sized ones in low X-ray energy ranges. More precisely, in high X-ray energies, almost no significant differences were observed between the nano-sized and micro-sized particles with the same weight percentages. In 2018, Tekin *et al.* [8], investigated the influence of WO_3 and Bi_2O_3 additives in micro and nano scales on the radiation shielding properties of hematite-serpentine concrete (HSC). The results showed that the values of μ/ρ of nanoparticles were higher than those of micro-particles. In another research, the attenuation of nano lead oxide and EPDM composite was investigated for development of polymer-based radiation shielding material. The nano-sized lead oxide showed improvement in regard to the radiation shielding behavior of the EPDM material [9].

The most important advantages of the nano-sized particles on the X-ray shielding properties of the materials are the maximization of surface to volume ratio and their high dispersion properties on the substrate. Both of these factors increase the surface electron density of the shield material, and therefore, raise the interaction probability of the impinged photons with the shield electrons which consequently leads to improving the shielding effectiveness [4-11].

There are several reports of experimental and theoretical studies on X-ray radiation shielding with the usage of various materials; however, among all of the candidate materials, lead has long been considered as a highly effective material for X-ray radiation attenuation owing to its high density [1-3, 12]. Lead is available in a variety of forms such as bricks, sheets and plates. Several recent studies considered the effect of the lead nanoparticles as a filler loading component for enhancing the shielding properties of other materials including polymers, composites, etc. [13-21]. Despite these investigations, the features of the pure nanostructured lead thin films have never been considered and evaluated. Additionally, shielding properties of nanostructured materials around the electron shell energy ranges have not been adequately assessed. As the use of lead thin

films in radiation shielding is a promising way for the development of X-ray radiation protection, this work focused on investigation of lead shielding properties. More precisely, in the present research, the investigation of the X-ray radiation shielding of thin lead films in the case of both the nano and bulk-structured samples were considered. Importantly, the impact of the material thickness and X-ray energy on the shielding properties of thin lead films was evaluated. The main novelties of this research can accordingly be considered as: determination of the X-ray shielding properties of nanostructured thin lead films for the first time; investigation of the effect of different X-ray energies and thicknesses on the shielding properties of the films; and finally comparison of the results between the nanostructured and bulk-structured samples.

In the following section, the theoretical and computational aspects of the X-ray radiation shielding properties of materials in addition to the sample preparation and characterization are presented in details. Then, theoretical and experimental results regarding the irradiation of the nanostructured and bulk-structured thin lead films have been considered. After that, a detailed discussion regarding the obtain results have been presented. The last section is devoted to the conclusion of this study.

MATERIALS AND METHODS

Theoretical methodology

When a mono energy X-ray with an intensity of I_0 incidents on the absorber with a thickness of x, the shielding ratio of the absorber can be considered as shown in equation 1 [2, 3, 12]:

$$1 - \frac{I}{I_0} = 1 - e^{-N\sigma_t x}. \tag{1}$$

Where N and σ_t indicate the atomic number density and total photon microscopic cross section, respectively. The energy spectrum of X-ray photons emitted from an X-ray generating tube has different characteristic X-ray lines that are superimposed on the continuous

264

Int. J. Radiat. Res., Vol. 18 No. 2, April 2020

bremsstrahlung spectrum. Regarding the fact that the microscopic cross-section is considerably dependent on the incident photon energy, calculations of the shielding ratio of the X-ray spectra are a difficult and laborious issue. The Monte-Carlo photon transport calculation code is an internationally recognized code for analyzing such complex computational problems, which are presented in the following.

MCNPX modeling and simulation

MCNPX code version 2.6 is employed to investigate the shielding ratio of the deposited lead thin films for different X-ray energies and material thicknesses. This code is based on the probabilistic transport Monte Carlo method as developed by the Los Alamos National Laboratory [22]. Printed with each tally bin is the relative error of the tally corresponding to one standard deviation. These errors cannot be believed reliable (hence, neither can the tally itself) unless the error is fairly low (below 5%). Additionally, MCNP performs a series of statistical tests to determine the statistical validity and convergence of tally scores and uncertainties. Tally fluctuation charts are printed to show how a tally mean, error, variance of the variance (an estimate of the error of the relative error), and slope of the largest history scores (the estimated exponent of the probability density function) fluctuate as a function of the number of histories run. MCNP additionally calculates a figure of merit (FOM)

for one tally bin of each tally as a function of the number of histories and prints the results in the tally fluctuation charts at the end of the output. The FOM should be approximately constant as the number of histories increases [22-25].

Sample preparation

High-pure commercial lead powder with the particle size smaller than 100 micrometers is supplied by the Merck Company to be used in this investigation. The lead thin films were fabricated with a different thickness of 10, 100 and 1000 nanometers using the Physical Vapor Deposition technique (PVD) [26]. The standard borosilicate thin cover slips with the thickness of approximately 130 micrometers were used as the substrate. The lead nanoparticles were deposited on the substrates with the deposition rate of 1 angstrom/s.

Sample characterization
Energy Dispersive X-ray Spectroscopy Analysis

The aim of the Energy Dispersive X-ray Spectroscopy Analysis (ESD) was to investigate the purity of the prepared samples. The importance of this analysis is laid upon the fact that any undesirable impurities can remarkably impact the experimental results. Figure 1 illustrates the EDS spectra of the samples by providing information on the different lead electronic shells in addition to the absence of any impurities.
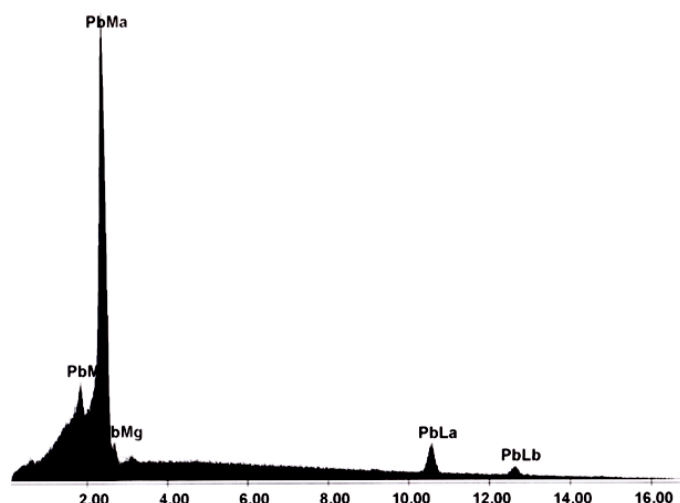

Figure 1. Measurement of lead purity using Energy Dispersive Spectroscopy (EDS).

Int. J. Radiat. Res., Vol. 18 No. 2, April 2020

265

Scanning electron microscopy observations

To make sure the accuracy of the measured thickness by the PVD technique, the Scanning Electron Microscopy (SEM) (KYKY model EM 3200) was employed. Figure 2 shows the cross face view of the sample 100 nm and 1000 nm thicknesses. As is shown, the thickness measured by the SEM technique is in good agreement with those obtained by the PDV technique.

Figure 3 shows the SEM images of the surface morphology for all of the fabricated lead thin films (i.e., 10, 100 and 1000 nm thicknesses). As is shown, agglomeration is occurred both for the samples of 100 nm and 1000 nm thicknesses; however, for the sake of comparison, it is much more evident for the latter case. Moreover, it is worth pointing out that the nano lead particles are distributed much more uniformly for the sample of 10 nm thickness than the other ones. Considering these observations, it seems that increasing the thickness of deposited lead films causes an increase in the agglomeration probability of nano lead particles which eventually leads to the reduction of surface electron density.

Theoretical and experimental results
Validation and benchmarking

Firstly, for a consistent and accurate comparison between the experimental measurements and the simulation results, the same set up was considered according to figure 4. In this analysis, the shielding ratio of a bulk lead sheet with the thickness of 60 micrometers for both the experimental and simulation measurements was obtained and then compared with each other in different X-ray energies.
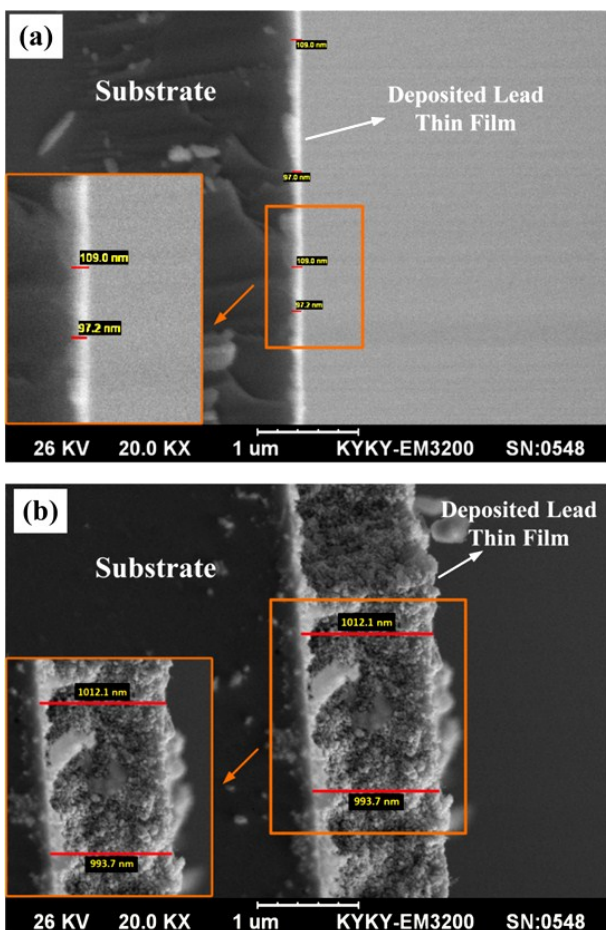

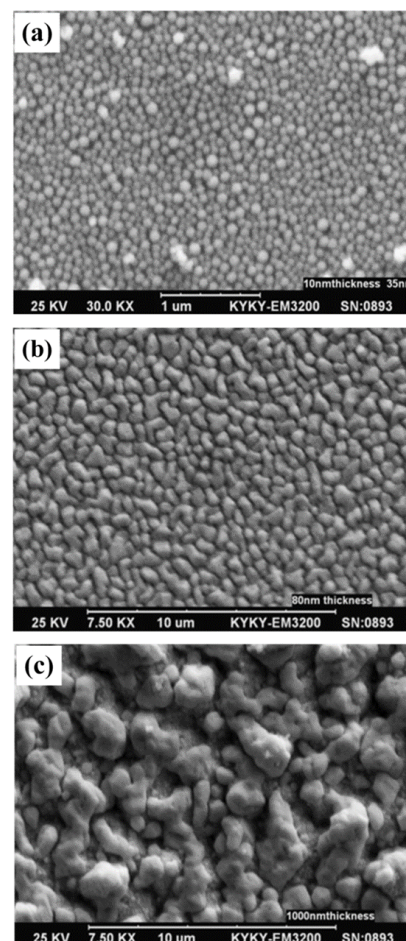**Figure 2.** Cross face view of a) 100 nm and b) 1000 nm thickness of deposited lead thin film.

Figure 3. SEM images of **a)** 10 nm, **b)** 100 nm and **c)** 1000 nm thickness of the deposited lead thin film.

266

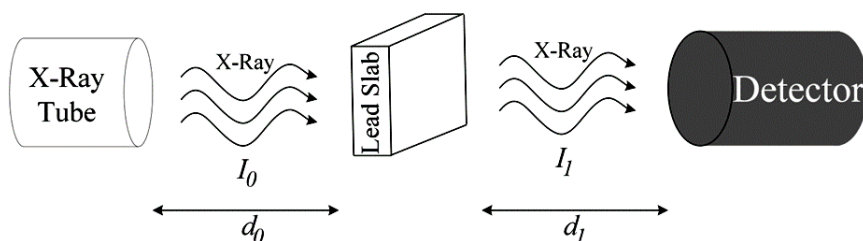*Int. J. Radiat. Res., Vol. 18 No. 2, April 2020*

Figure 4. Schematic view of the experimental and simulation setups for benchmarking.

Figure 4 shows the simplified geometry configuration of the X-ray generating tube which has been used as the input for the MCNPX code. As can be observed, d_0 is the distance from the X-ray window and the lead slab, and d_1 is the distance from the lead slab and the detector. In order to consider the highest possible number of the transmitted and scattered photons, both d_0 and d_1 are considered to be less than 0.5 mm. As is shown, the X-ray generation is the first thing that should be obtained. Accordingly, a mono-energy electron beam was designed to impinge on the copper target with a 45° angle, and then the beryllium window was considered to be located at the 90° angle to the incident electron beam. The thickness and density of the beryllium window were assumed to be 125 microns and 1.85 g/cm³, respectively.

The X-ray spectra were determined by F1: p tally of MCNPX code and then the shielding ratio of the lead slab were obtained in different X-ray energies based on a combination of X-ray spectrum and energy-dependent attenuation coefficients. The configuration of the detector considered as the manufacturer design and

information so that the density of Mica window, the diameter of the housing, the diameter of the counter tube and counter tube length are 1.75 (mg / cm²), 22 mm, 15 mm and 76 mm, respectively. Additionally, it should be noted that the impact of detector's dead time on the results has been considered. The sample size was considered to be 22×22 mm to properly be fitted the window of the counter tube.

To compare the experimental and theoretical results, the Apparent Absolute Error (AAE) in shielding ratio was calculated using equation 2 [27, 28]:

AAE (%) = |Theoretical Vallue - Experimental Vallue| × 100   (2)

High-pure commercial lead slab, purchased from the Hopkins and Williams Company, was used in this section of work as the absorber for validation and benchmarking. The thickness of the slab was 60 micrometers and the results all tabulated in table 1 for different irradiated X-ray energy voltage peaks.

Table 1. Theoretical and experimental results of the shielding ratio for 60 micrometer bulk Lead sheet.

Energy (keV)	Theoretical result (%)	Experimental result (%)	AAE (%)
8	99.81	99.79	1.89
9	99.76	99.74	1.70
10	99.65	99.63	1.50
11	99.40	99.39	1.43
12	99.13	99.12	1.28
13	98.69	98.68	1.12
14	98.14	98.13	0.75

As is shown, the MCNPX computational measurements are in good agreement with those obtained from the experiments.

Irradiation characterization

A typical X-ray tube (commercial RONTGENGERAT German type X-ray tube) with

Int. J. Radiat. Res., Vol. 18 No. 2, April 2020

267

a target of copper was used to consider and characterize the X-ray shielding property of thin lead films. The tube currently in use can be set in the ranges 8 keV toward the 14 keV (due to the long-life of the tube). The built-in rate meter including counter-tube voltage supply enables direct measuring of photons using a Geiger-Muller counter tube. The employed Geiger Mueller tube (PHYWE model 09025-11) was considered to count the transmitted X-ray radiations; however by considering the detector's dead time effect.

In this work, three lead samples with a different thickness of 10, 100 and 1000 nm were considered to investigate a wide range of thickness variations. As is shown in figure 5, each sample is located between the Geiger Mueller counter and the X-ray tube.

In order to obtain the shielding ratio of the nanostructured and bulk-structured thin lead films, firstly, the transmission of X-rays from the substrate has been determined. As is illustrated in figure 5(a), firstly, the number of transmitted X-rays from the substrate is counted and then the aforementioned lead samples are located between the counter and X-ray source. Figure 5 (b) and (c) show the schematic view of the experimental and theoretical setup, respectively.
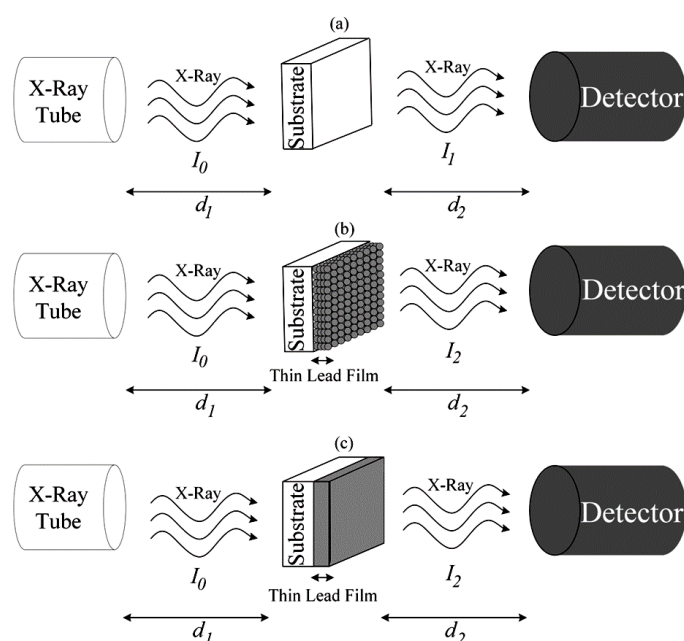
Figure 5. Schematic view of the irradiated and transmitted X-ray radiations **a)** through substrate **b)** through both substrate and thin lead film for the experimental setup **c)** through both substrate and thin lead film for the MCNPX setup.

Where; d_0 is the distance between the X-ray tube and the substrate and d_2 is the distance between the lead film and the detector. Similar to the previous experiment, the sample size was considered to be 22×22 mm to properly fit the window of the counter tube. It should be noted that each experiment was repeated 20 times. Regarding figure 5 and using equation(2), the shielding ratio of the experimental and theoretical measurements was calculated for different X-ray energies ranging from 8 to 14 keV using equation 3:

$$Shielding\ Ratio(\%) = (1 - \frac{I_2}{I_1}) \times 100, \qquad (3)$$

Where; I_1 and I_2 are the transmitted X-rays from the substrate and from both substrate and thin lead films, respectively. The experimental and theoretical MCNPX results have been presented in figure 6. It should be noted that the required corrections to the experimental data due to the detector's dead time effect have been applied. Moreover, to reduce the counting uncertainty, the number of performed counts

268

Int. J. Radiat. Res., Vol. 18 No. 2, April 2020

and the acquisition time used in each measurement are considered to be 50 times and 120s, respectively.

Form a simulation point of view, the statistical uncertainty of the results based on the MCNPX code has been considered. It has been shown that all of the 10 statistical checks for the tally fluctuations have been passed. To be more precise, all of the results have a fewer relative error of 2.0%, fewer Variance Of Variance (VOV) of 0.0001, near-constant large value and random behavior of FOM and finally constant slope value of 10.0.

To investigate the X-ray shielding ratio of the nanostructured and bulk-structured thin lead films versus thickness variations, the following results (figure 7) regarding the experimental and theoretical calculations are illustrated.
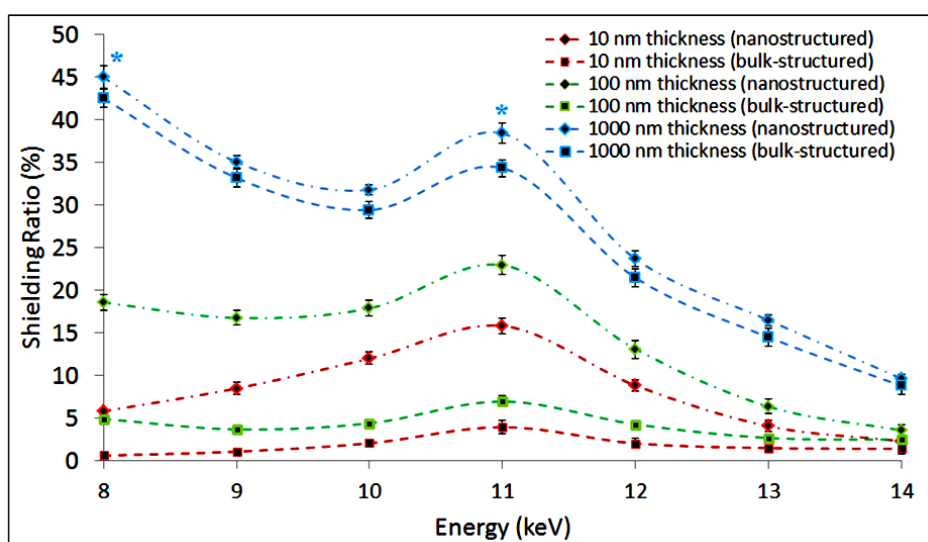

Figure 6. Shielding ratio comparison between the experimental and theoretical results for different X-ray energies.
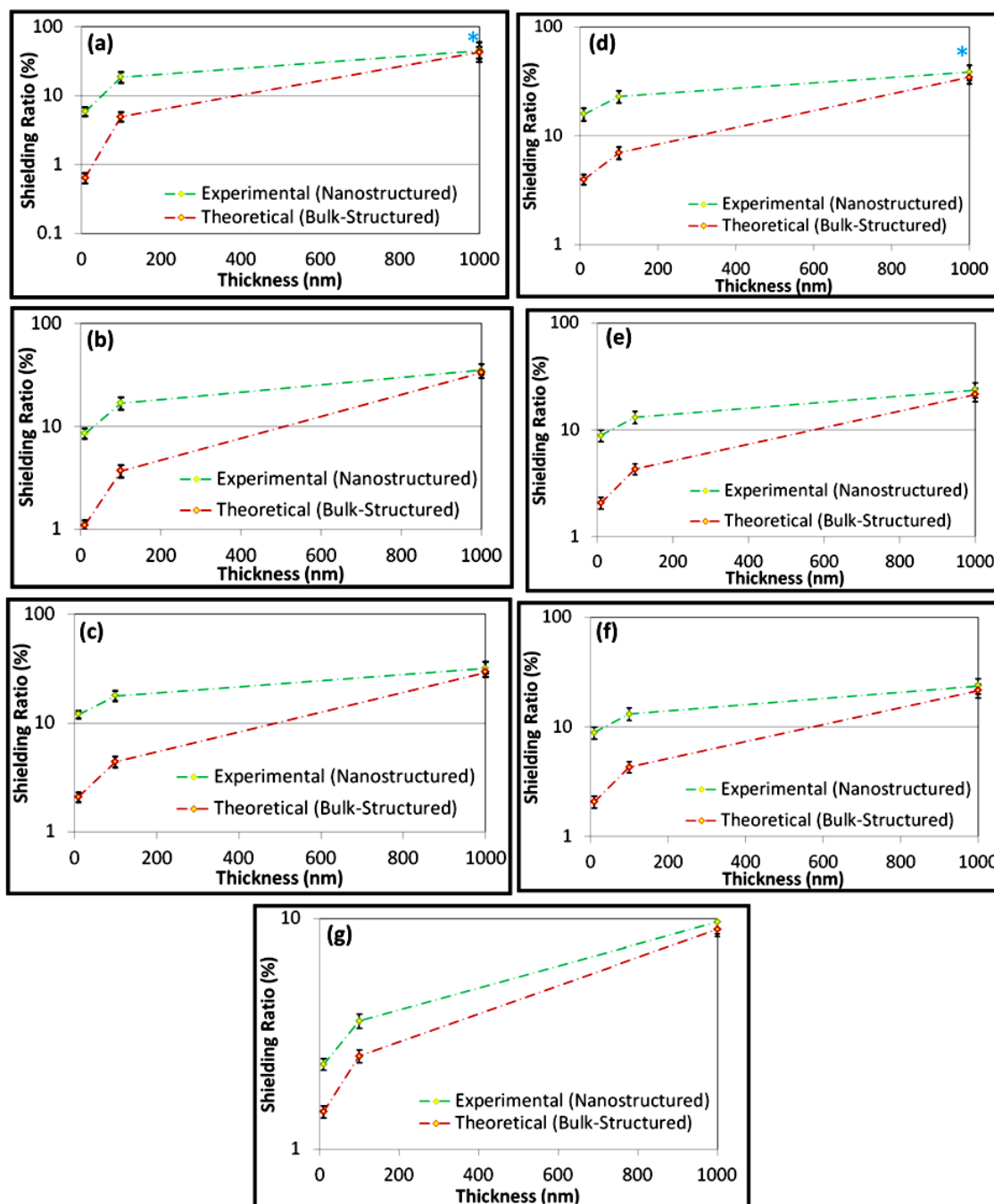
Int. J. Radiat. Res., Vol. 18 No. 2, April 2020

269

Figure 7. Shielding ratio of the deposited lead thin films for 8 keV **(a)**, 9 keV **(b)**, 10 keV **(c)**, 11 keV **(d)**, 12 keV **(e)**, 13 keV **(f)** and 14 keV **(g)** X-ray energy.

DISCUSSION

Figure 6 shows that the shielding ratio of the nanostructured thin lead films is significantly higher than those calculated from the bulk-structured for all lead thicknesses and impinged X-ray energy ranges. This result is almost the same as the result already obtained by other researchers with different materials [4-9]. More precisely, in the case of WO_3, Noor Azman *et al.* [4 and 5], confirmed the superior attenuation ability of nano-sized WO_3-epoxy composites than they predicted. A similar result also was observed by Mesbahi and Ghiasi [6] and

270

Int. J. Radiat. Res., Vol. 18 No. 2, April 2020

they showed a higher photon attenuation coefficient of nano-sized particles of PbO_2, Fe_2O_3, WO_3 and H_4B (Boronium) compared to the larger particle sizes. In the case of CuO, Kunzel and Okuno [7] also found that the X-ray absorption is higher for the nanostructured samples compared to the microstructured samples for all CuO concentrations. By taking into account of these works and the results presented in figure 7 for the lead material, one can reasonably argue that the results herein are consistent with those obtained by the other researchers. In fact, it has been shown that the shielding property of materials is increased only by nanosizing the particles. This superiority of the nanostructures; however, is more evident for the small thicknesses. In fact, the results indicate that the difference of the determined shielding ratio between the two structures decreases with increasing the lead thickness in almost each incident X-ray energy. The main reason for these observations can be explained by considering figure 3, in which the agglomeration of the nanoparticles was raised by increasing the thickness considerably. On this basis, the maximization of the surface to volume ratio, which is normally occurred by nanosizing the particles, will be decreased. This leads to the reduction of surface electron density and, eventually, reduction of the reaction rate of electrons with incident photons. This part of the results did not well investigate by other researchers even for other materials. This is due to the fact that the nano particles usually were distributed in a matrix as a filler by different concentrations, and accordingly, the higher thicknesses did not cause the higher agglomeration. On this basis, a new finding of the effect of agglomeration on the shielding properties of the materials is revealed. According to figures 3 and 6, the agglomeration of the nano particles causes a reduction in the discrepancy of the shielding properties between the nanostructured and bulk-structured samples. This means that the shielding properties of the materials increase by increasing the thickness of the shield in the case of both nanostructured and bulk-structured samples, however, the superiority of the

nanostructured thin lead films is reduced due to the agglomeration effect. This new aspect of the shielding properties of the nano materials has not been investigated previously mostly due to the fact that in all the previous studies the nano particles only have been employed as the additive component. For instance, Özdemir *et al.* [9] showed that the photon attenuation of EPDM increases consistently by increasing the thickness of the samples that contain PbO nanoparticles as the additive component. Similar results also were obtained in the case of other additive materials including PbO_2, PbO, and $PbTiO_3$ [13], WO_3 [4,5], Fe_2O_3 [6] and CuO [7]. However, according to our results, it can be revealed that not only the thickness of the shield but also the agglomeration effect of the nano particles is of great importance in X-ray shielding.

From a different point of view, figure 6 also shows that the difference between the nanostructured and bulk-structured thin lead films diminished by raising the X-ray energy in all sample thicknesses and was finally eliminated at 14 keV. These results are consistent with those obtained by previous works which showed a higher attenuation ability of the nano-sized particles than those of the micro-sized particles in low X-ray energy ranges (Noor Azman *et al.* for the energy range investigation of 10-40 keV [4] and also 22-120 keV [5] using WO_3 nano particles, and also for the energy range investigation of 40-100 keV using W, Au and Pb nano particles [11], Mesbahi and Ghiasi for the energy range investigation of 142-1250 keV using PbO_2, Fe_2O_3, WO_3 and H_4B nano particles [6], Kunzel and Okuno for the energy range investigation of 25-120 keV using CuO nano particles [7], and Tekin *et al.* for the energy range investigation of 0.142–1.33 MeV using WO_3 and Bi_2O_3 nano particles [8]. This is due to the fact that the photon interaction probability decreases by increasing the incident photon energy, therefore, the superiority of the nanostructured samples which is due to the very high interactions of the incident photons with the electrons in the thin films are affected and eventually reduced. This leads to the almost similar number of interactions between the

Int. J. Radiat. Res., Vol. 18 No. 2, April 2020

271

incident photons and electrons in the thin lead films, and consequently, similar shielding properties of the nanostructured and bulk-structured samples in the same high X-ray energies. Another important point is that the nano and bulk-structured samples both have a sharp value around 11 keV in all lead thicknesses. This may be due to the existence of an electron shell in the lead material around 11 keV which was also observed previously by EDS spectra in figure 1. In fact, because, in this study, the X-ray energy range variations are 8 keV to 14 keV, the dominant interaction is, therefore, photoelectric, and consequently, the existence of an electron shell around 11 keV can lead to increasing the interaction probability and shielding ratio. This result can be very important from the point of view of shielding properties of nanostructured materials around the electron shells energy ranges. This observation is important also, because, in almost all of the previous works, the shielding properties of the nano materials were mostly investigated in much higher energy ranges than those considered in this work, and, accordingly, the behavior of nanostructured materials in low X-ray energies was unclear [5-9]. For instance, Noor Azman *et al.* studied the energy range of 22 -120 keV [5] and also 40-100 keV [11], Mesbahi and Ghiasi considered the energy range of 142-1250 keV [6], and Tekin *et al.* investigated the energy range of 0.142–1.33 MeV [8]. Among all of the previous studies, a recent work on WO_3 -filled epoxy composites [4] considered the energy range investigation of 10-40 keV. According to their results, it was shown that the X-ray transmission is lower around 10 keV compared to higher X-ray energies. Although this observation did not explain and investigate in their work, it can be considered and explained according to our results. We have found that tungsten has an electron shell around 10 keV [29] and this is the reason for observation a higher X-ray attenuation in their work at 10 keV X-ray energy. Based on these results, it can reasonably be argued that the results of our work (for the Lead material) is consistent with those obtained by Noor Azman *et al.* [4] (for WO_3).

Another important result that can be obtained from figure 6 is that the nanostructured sample with the thickness of 10 nm has higher shielding properties compared to the bulk-structured sample with the thickness of 100 nm. This is an important observation that shows the effectiveness of the nanostructured thin lead films compared to the bulk-structured films even at different thicknesses. In other words, the low thickness of the nanostructured thin lead films can even be more effective than ten times more thick bulk-structured samples at the same X-ray energies.

In figure 6, also, Standard Deviation (SD) of the expermental measurments and theoretical calculations are presented. As can be observed, the theoretical SD is almost the same for different measurments. This is due to the fact that the SD in the theoretical calculations using the MCNPX code always kept below a certain value and if it exceeded, the calculations were again performed with more execution time and number of particle histories. Despite the theoretical calculations, SD is different regarding the number of recorded radiations in the detector and the number of repetition of the measurements.

The first thing that will be cleared from figure 7 is that, the shielding ratio for both nanostructured and bulk-structured thin films increases with increasing the thickness of lead layers in all incident X-ray energies due to the raising the fraction of deposition X-ray energies by growing the thickness of the shield. According to the results, it is also possible to observe that, the form of variations is in the form of Eq. (3) for both the aforementioned structures. However, the shielding ratio of the nanostructured films in all X-ray energies is significantly higher than of bulk-structured films, particularly for both samples of 10 and 100 nm thicknesses. In the case of 1000 nm lead thickness; however, the measured data almost reached to each other. Based on this argument, it may be inferred that by increasing the lead thickness, the difference between the nanostructured and bulk-structured lead thin films tends to be diminished. The most obvious explanation for this observation might be due to the agglomeration phenomenon. In fact, as is

shown in figure 3 and explained previously, the agglomeration of the deposited lead thin films increases with increasing the shield thickness remarkably. So, the surface electron density which was the main reason for the superiority of the nanostructured over the bulk-structured thin films will decrease. This leads to the reduction of the interaction probability between the incident photons and the lead electrons and consequently leads to the reduction of difference in the results. In figure 7, additionally, SD of the experimental measurments and theoretical calculations are shown. Similar to figure 6, SDs of the theoretical calculations are almost the same as each others. However, in the case of experimental measurments, the number of recorded radiations in the detector and the number of repetition of the measurments are the main reasons for the discrepancy between the obtained results. From the point of view of making a comparison, as it is observable in figures 6 and 7, the SDs in 8 keV and 11 keV for the 1000 nm thickness (with the blue sign of * in figures 6 and 7) have the most discrepancy not only between experimental measurements but also between the experimental measurements and theoretical calculations. This is due to the fact that the shielding ratio is higher in these two energies. The higher shielding ratio leads to the lower recorded signals in the detector and eventually the higher SDs in the experimental measurements. When it compares to the theoretical calculations (which have almost the same SDs as explained previously), these discrepancies also are again observable at these two energies.

Regarding the above discussion, it can be concluded that, for low energy X-ray s (8-14 keV), the nanostructured thin lead films attenuate photons more compared to the bulk-structured films with the same thicknesses. However, the discrepancy disappears as film thickness increases to 1000 nm or the X-ray energy reaches 14 keV.

CONCLUSION

In this study, investigation of the X-ray

shielding properties of bulk and nanostructured thin lead films was performed by means of Monte-Carlo calculations and experimental measurements. The results revealed that, for low energy X-ray s, the nanostructured thin lead films attenuate more than bulk-structured samples; however, the difference disappears as film thickness increases to 1000 nm or the X-ray energy reaches 14 keV.

Conflicts of interest: *Declared none.*

REFERENCES

1. Knoll GF (2000) Radiation detection and measurement. John Wiley and Sons, Inc. New York.
2. Meyerhof WE (1967) Elements of nuclear physics. McGraw-Hill, New York.
3. Johns HE and Cunningham JR (1983) The physics of radiology. Charles C Thomas, Illinois.
4. Noor Azman NZ, Siddiqui SA, Low IM (2013) Characterisation of micro-sized and nano-sized tungsten oxide-epoxy composites for radiation shielding of diagnostic X-rays. *Mat Sci Eng C*, **33**: 4952-4957.
5. Noor Azman NZ, Siddiqui SA, Hart R Low IM (2013) Effect of particle size, filler loadings and X-ray tube voltage on the transmitted X-ray transmission in tungsten oxide epoxy composites *Appl Radiat Isot,* **71**: 62-67.
6. Mesbahi A and Ghiasi H (2018) Shielding properties of the ordinary concrete loaded with micro- and nano-particles against neutron and gamma radiations. *Appl Radiat Isot*, **136**: 27-31.
7. Kunzel R and Okuno E (2012) Effects of the particle sizes and concentrations on the X-ray absorption by CuO compounds. *Appl Radiat Isot,* **70**: 781-784.
8. Tekin HO, Sayyed MI,.Issa SAM (2018) Gamma radiation shielding properties of the hematite-serpentine concrete blended with WO_3 and Bi_2O_3 micro and nano particles using MCNPX code. *Radiat Phys Chem,* **150**: 95-100.
9. Özdemir T, Güngör A, Akbay IK, Uzun H, Babucçuoglu Y (2018) Nano lead oxide and epdm composite for development of polymer based radiation shielding material: Gamma irradiation and attenuation tests. *Radiat Phys Chem,* **144**: 248-255.
10. Vagheian M, Saramad S, Rezaei-Ochbelagh D, Sardari D (2017) On an experimental study of the electron generation property of thin gold films. *J Chem,* **6**: 84-92.
11. Noor Azman NZ, Siddiqui SA, Ionescu MR Low IM (2012) Synthesis and characterisation of ion-implanted epoxy composites for X-ray shielding. *Nucl Instrum Methods Phys Res Sec B,* **287**: 120-123.
12. Chilton AB, Shultis JK, Faw RE (1984) Principles of radiation

Int. J. Radiat. Res., Vol. 18 No. 2, April 2020

273

shielding. Prentice-Hall, Inc, Englewood Cliffs.

13. Hassan HE, Badran HM, Aydarous A, Sharshar T (2015) Studying the effect of nano lead compounds additives on the concrete shielding properties for γ-rays. *Nucl Instr Meth Phys Res B*, **360**: 81-89.

14. Alwaeli M (2017) Investigation of gamma radiation shielding and compressive strength properties of concrete containing scale and granulated lead-zinc slag wastes. *J Clean Prod*, **166**: 157-162.

15. Zhang X, Yang M, Zhang X, Wu H, Guo S, Wang Y (2017) Polymer-Composite materials for radiation protection. *Compos Sci Technol*, **150**: 16-23.

16. Mondala S, Gangulya S, Dasb P, Bhawala P, Dasa TK, Ravindrena R, Ghosha S, Dasa NCh (2017) Effect of thermal-air ageing treatment on mechanical properties and electromagnetic interference shielding effectiveness of low-cost nano-structured carbon filled chlorinated polyethylene. *Mater Sci Eng B*, **225**: 140-149.

17. La LBT, Leong Y, Leatherday C, Au PI, Haywarda KJ, Zhang L (2016) X-ray protection, surface chemistry and rheology of ball-milled submicron Gd2O3 aqueous suspension. *Colloids Surf A*, **501**: 75-82.

18. Rezaei-Ochbelagh D and Azimkhani S (2012) Investigation of gamma-ray shielding properties of concrete containing different percentages of lead. *Appl Radiat Isot*, **70**: 2282-2286.

19. Kim J, Seo D, Lee BC, Seo YS, Miller WH (2014) Nano- W dispersed gamma radiation shielding materials. *Adv Eng Mater,* **16**: 1083-1089.

20. Botelho MZ, Kunzel R, Okuno E, Levenhagen RS, Basegio T, Bergmann CP (2011) X-ray transmission through nanostructured and microstructured CuO materials. *Appl Radiat Isot,* **69**: 527-530.

21. Adliene D, Cibulskaite I, Meskinis S (2010) Low energy X-ray radiation impact on coated Si constructions. *Radiat Phys Chem,* **79**: 1031-1038.

22. MCNPX user's manual version 2.6.0 (2008). Los Alamos National Laboratory.

23. Briesmeister JF (1986) MCNP: a general Monte Carlo code for neutron and photon transport version 3A. Los Alamos National Laboratory.

24. Shultis JK and Faw RE (2011) An MCNP primer. Kansas State University.

25. Kiedrowski BC and Solomon CJ (2011) Statistical assessment of numerous Monte Carlo tallies. *International Conference on Mathematics and Computational Methods*, Brazil, ISBN 978-85-63688-00-2.

26. Mahan JE (2000) Physical vapor deposition of thin films. John Wiley & Sons, New York, ISBN 0-471-33001-9.

27. Vagheian M, Rezaei Ochbelagh D, Gharib M (2016) An improved box-scheme finite difference method based on the relative event probabilities. *Prog Nucl Energy*, **88**: 33-42.

28. Vagheian M, Vosoughi N, Gharib M (2016) Enhanced finite difference scheme for the neutron diffusion equation using the importance function. *Ann Nucl Energy,* **96**: 412–421.

29. Bearden JA and Burr AF (1967) Reevaluation of X-ray atomic energy levels. Rev Mod Phys, **39**: 125.

274

Int. J. Radiat. Res., Vol. 18 No. 2, April 2020